Journal of Applied Fluid Mechanics, Vol. 9, No. 1, pp. 215-223, 2016.
Available online at www.jafmonline.net, ISSN 1735-3572, EISSN 1735-3645.
DOI: 10.18869/acadpub.jafm.68.224.24042

Three-Dimensional MHD Flow of Casson Fluid in Porous Medium with Heat Generation

S. A. Shehzad[1†], T. Hayat[2,3] and A. Alsaedi[3]

[1.] *Department of Mathematics, Comsats Institute of Information Technology, Sahiwal 55000, Pakistan*
[2.] *Department of Mathematics, Quaid-i-Azam University 45320, Islamabad 44000, Pakistan*
[3.] *Department of Mathematics, Faculty of Science, King Abdulaziz University, P.O. Box 80257, Jeddah 21589, Saudi Arabia*

†*Corresponding Author Email: ali_qau70@yahoo.com*

(Received September 10, 2014; accepted November 17, 2014)

ABSTRACT

The magnetohydrodynamic (MHD) three-dimensional boundary layer flow of an incompressible Casson fluid in a porous medium is investigated. Heat transfer characteristics are analyzed in the presence of heat generation/absorption. Laws of conservation of mass, momentum and energy are utilized. Results are computed and analyzed for the velocities, temperature, skin-friction coefficients and local Nusselt number.

Keywords: Three-dimensional flow; Casson fluid; Stretching surface; Heat generation/absorption.

NOMENCLATURE

u, v, w	velocity components	σ^*	electrical conductivity
β	Casson parameter	K	permeability parameter
ρ	fluid density	ν	kinematic viscosity
T	temperature	B_0	Applied magnetic field
σ	thermal diffusivity	Q	heat generation parameter
c_p	specific heat	T_∞	ambient fluid temperature
f, g	dimensionless velocity components	θ	dimensionless temperature
M	Hartman number	λ	porosity parameter
α	ratio parameter	Pr	Prandtl number
B	heat source/sink parameter	τ_{wx}	wall shear stress
q_w	wall heat flux		

1. INTRODUCTION

The magnetohydrodynamic (MHD) flows of an electrically conducting fluid are encountered in many geophysical, astrophysical and engineering applications. Hydromagnetic flows have a key role in the fields of aeronautics, stellar and planetary magnetospheres. Magnetohydrodynamics concepts are utilized by the engineers in the design of heat exchangers, pumps, thermal protection, in space vehicle propulsion, control and re-entry, and in creating novel power-generating systems. The purification of molten metals from non-metallic inclusions through the application of magnetic field is another important feature of MHD. All such applications of MHD give rise to investigate the problems which involves the magnetohydrodynamic effects. For example, Turkyilmazoglu (2011) studied MHD boundary layer flow of viscous fluid over a rotating sphere near an equator with heat transfer. He presented both numerical and analytical solutions. MHD boundary layer flow of viscous fluid induced by an exponentially shrinking sheet was studied by Bhattacharyya and Pop (2011). Makinde (2012) examined MHD boundary layer flow of viscous fluid over flat surface with Newtonian heating and Navier slip. Hayat *et al.* (2012a) developed the series solution for the MHD flow of an Oldroyd-B fluid passing through a porous channel. Rashidi and Mehr (2014) considered problem for the series solutions of velocity and temperature. On the other hand the flows in porous media have practical applications in heat removal from nuclear fuel

debris, underground disposal of radiative waste material, storage of food stuffs, paper production, oil exploration etc. Especially, the related boundary layer flows with heat transfer have received much attention of the researchers in view of achieving industrial product of desired quality. The rates of cooling and stretching have key role in such situations. No doubt, the flow generated by the stretching of a flat surface has a great relevancy to the polymer extrusion. For example, the extrudite from the die is generally drawn and simultaneously stretched into a surface in a melt spinning process, which is thereafter solidified through rapid quenching or gradual cooling by direct contact water or chilled metal rolls. Closed form solution for the boundary layer flow of viscous fluid over a stretching surface was firstly constructed by Crane (1970). He assumed that the stretching surface possess a linear velocity with fixed distance from the origin. Afterwards the Crane's problem has been studied extensively through different aspects (see few recent studies for two-dimensional flows (Rashidi *et al*. (2011), Javed *et al*. (2011), Mukhopadhyay (2012) and Hayat *et al*. (2012b)).

It is well known fact that the fluids appear in industrial and engineering processes are mostly non-Newtonian fluids. There are materials like drilling muds, sugar solution, certain oils, clay coating, colloidal and suspension solution, certain oils, lubricants etc. which fall into the category of non-Newtonian fluids. The properties of such materials cannot be explored by simple Navier-Stokes equations. According to the diverse characteristics of such materials, different fluid models are developed in the past like second grade fluid (Jamil *et al*. (2011)), third grade fluid (Abelman *et al*. (2009)), fourth grade fluid (Hayat *et al*. (2010)), Maxwell and Oldroyd-B fluids (Wang and Tan (2011) and Jamil *et al*. (2014)), Burgers' fluid (Jamil and Fetecau (2010)), Jeffrey fluid (Hayat *et al*. (2012c)), Eyring-Powell fluid (Hayat *et al*. (2014a)), micropolar fluid (Rashidi *et al*. (2011)), Walters' B fluid (Hayat *et al*. (2014b)), Casson fluid (Shahmohamadi (2012)) etc. The fluid model under consideration is Casson. This model is plastic fluid model that exhibits the characteristics of shear thinning that quantifies the yield stress and high shear viscosity. This fluid model is a good candidate to explore the properties of biological materials, foams, molten chocolate, cosmetics, nail polish etc.

Previous literature on the topic witnesses that little has been said yet about the three-dimensional flows. There are only few attempts in this direction. For example, Wang (1984) investigated the three-dimensional boundary layer flow of viscous fluid generated by linearly stretched surface. Hydromagnetic three-dimensional free convection flow over a stretching surface was studied by Chamkha (1999). Ariel (2003) provided the homotopy perturbation solution of the problem of Wang (1984). Shehzad *et al*. (2012) discussed the three-dimensional boundary layer flow of Jeffrey fluid with convective conditions. The aim here is to develop a mathematical model for three-dimensional flow of Casson fluid over a linearly stretching surface. The magnetohydrodynamic fluid fills the half space. Further, heat transfer effects are taken into account when heat generation/absorption effects are present. The governing nonlinear partial differential equations are converted into the ordinary differential equations by employing suitable transformations. The resulting nonlinear is computed by a newly developed modern technique namely the homotopy analysis method (Liao (2003), Rashidi and Erfani (2012), Hayat *et al*. (2012b), Turkyilmazoglu (2012), Shehzad *et al*. (2013), Shehzad *et al*. (2014), Hayat *et al*. (2014c,d) and Malvandi *et al*. (2014a,b) (HAM). Results are plotted and displayed. The important observations of this study are listed in the conclusions.

2. MATHEMATICAL FORMULATION

We consider three-dimensional boundary layer flow of an incompressible Casson fluid in a porous medium. The fluid is electrically conducting under the influence of a constant applied magnetic field $\mathbf{B}_0$. In addition, the induced magnetic field is not considered because of small magnetic Reynolds number. Physical properties of fluid are assumed constants. Effects of viscous dissipation are neglected. Mathematical formulation is given in the presence of heat generation/absorption. We denote u, v and w the x, y and z components of velocity, T the temperature and T_∞ the ambient temperature, respectively. The resulting boundary layer equations are

$$\frac{\partial u}{\partial x}+\frac{\partial v}{\partial y}+\frac{\partial w}{\partial z}=0, \tag{1}$$

$$u\frac{\partial u}{\partial x}+v\frac{\partial u}{\partial y}+w\frac{\partial u}{\partial z}=\nu\left(1+\frac{1}{\beta}\right)\frac{\partial^2 u}{\partial z^2} -\frac{\sigma^* B_0^2}{\rho}u-\frac{\nu}{K}u, \tag{2}$$

$$u\frac{\partial v}{\partial x}+v\frac{\partial v}{\partial y}+w\frac{\partial v}{\partial z}=\nu\left(1+\frac{1}{\beta}\right)\frac{\partial^2 v}{\partial z^2} -\frac{\sigma^* B_0^2}{\rho}v-\frac{\nu}{K}v, \tag{3}$$

$$u\frac{\partial T}{\partial x}+v\frac{\partial T}{\partial y}+w\frac{\partial T}{\partial z}=\sigma\frac{\partial^2 T}{\partial z^2} +\frac{Q}{\rho c_p}(T-T_\infty), \tag{4}$$

where $\beta=\mu_B\sqrt{2\pi_c}/p_y$ is the Casson fluid parameter, σ^* the electrical conductivity, K the permeability parameter, c_p the specific heat, σ the thermal diffusivity of the fluid, $\nu=(\mu_B/\rho)$ the kinematic viscosity, μ_B the plastic dynamic viscosity of Casson fluid, ρ the density of fluid

and Q the volumetric heat generation/absorption coefficient.

The corresponding boundary conditions are:

$$u = ax,\ v = by,\ w = 0,\quad T = T_w \ \text{ at } z = 0, \tag{5}$$

$$u \to 0,\ v \to 0,\ T \to T_\infty \ \text{ as } z \to \infty, \tag{6}$$

where the fluid temperature of the wall is T_w. Employing the transformations (Wang (1984) and Shehzad *et al*. (2012)):

$$u = axf'(\eta),\ v = ayg'(\eta),$$

$$w = -\sqrt{av}\,(f(\eta) + g(\eta))\ \theta(\eta) = \frac{T - T_\infty}{T_w - T_\infty},\ \eta = z\sqrt{\frac{a}{\nu}} \tag{7}$$

one obtains

$$\left(1+\frac{1}{\beta}\right)f''' + (f + g)f'' - f'^2 - \left(M^2 + \frac{1}{\lambda}\right)f' = 0, \tag{8}$$

$$\left(1+\frac{1}{\beta}\right)g''' + (f + g)g'' - g'^2 - \left(M^2 + \frac{1}{\lambda}\right)g' = 0, \tag{9}$$

$$\theta'' + \Pr(f + g)\theta' + \Pr B\theta = 0, \tag{10}$$

$$f = 0,\ g = 0,\ f' = 1,\quad g' = \alpha,\ \theta = 0 \ \text{ at } \eta = 0, \tag{11}$$

$$f' \to 0,\ g' \to 0,\ \theta \to 0 \ \text{ as } \eta \to \infty, \tag{12}$$

where Eq. (1) is satisfied automatically, $M^2 = \sigma^* B_0^2 / a\rho$ the Hartman number, $\lambda = \frac{Ka}{\nu}$ the porosity parameter, $\alpha = \frac{b}{a}$ is a ratio parameter, $\Pr = \frac{\nu}{\sigma}$ the Prandtl number, $B = Q / \rho a c_p$ the heat generation/absorption coefficient and prime depicts differentiation with respect to η.

If C_{fx} and C_{fy} are the skin-friction coefficients and Nu_x is the local Nusselt number, then we have

$$C_{fx} = \frac{\tau_{wx}}{\rho u_w^2},\ C_{fy} = \frac{\tau_{wy}}{\rho u_w^2},\quad Nu_x = \frac{xq_w}{k(T_w - T_\infty)}, \tag{13}$$

where τ_w and q_w are the wall shear stress and the wall heat flux, respectively. The above equation in dimensionless form can be written as

$$\mathrm{Re}_x^{1/2} C_{fx} = \left(1+\frac{1}{\beta}\right) f''(0),$$

$$\mathrm{Re}_x^{1/2} C_{fy} = \left(1+\frac{1}{\beta}\right) g''(0),$$

$$\mathrm{Re}_x^{-1/2} Nu_x = -\theta'(0), \tag{14}$$

where the definition of Reynolds number is $\mathrm{Re}_x = u_w(x)x / \nu$.

3. HOMOTOPY SOLUTIONS

According to HAM, the functions f, g and θ by a set of base functions

$$\{\eta^k \exp(-n\eta),\ k \ge 0, n \ge 0\}$$

can be expressed as

$$f_m(\eta) = \sum_{n=0}^{\infty}\sum_{k=0}^{\infty} a_{m,n}^k \eta^k \exp(-n\eta), \tag{15}$$

$$g_m(\eta) = \sum_{n=0}^{\infty}\sum_{k=0}^{\infty} b_{m,n}^k \eta^k \exp(-n\eta), \tag{16}$$

$$\theta_m(\eta) = \sum_{n=0}^{\infty}\sum_{k=0}^{\infty} c_{m,n}^k \eta^k \exp(-n\eta), \tag{17}$$

in where $a_{m,n}^k$, $b_{m,n}^k$ and $c_{m,n}^k$ are the coefficients. Initial approximations and auxiliary linear operators are given by

$$f_0(\eta) = \left(1 - e^{-\eta}\right),\ g_0(\eta) = \beta\left(1 - e^{-\eta}\right),\ \theta_0(\eta) = e^{-\eta},$$
$$L_f = f''' - f',\ L_g = g''' - g',\ L_\theta = \theta'' - \theta. \tag{18}$$

The operators have the following properties

$$L_f(C_1 + C_2 e^{\eta} + C_3 e^{-\eta}) = 0,$$
$$L_f(C_4 + C_5 e^{\eta} + C_6 e^{-\eta}) = 0,$$
$$L_\theta(C_7 e^{\eta} + C_8 e^{-\eta}) = 0, \tag{19}$$

in which C_i $(i = 1-8)$ show the arbitrary constants.

The zeroth order deformation problems can be obtained as:

$$(1-p)L_f\left[\hat{f}(\eta;p) - f_0(\eta)\right] = p\hbar_f \mathbf{N}_f\left[\hat{f}(\eta;p), \hat{g}(\eta;p)\right], \tag{20}$$

$$(1-p)L_g\left[\hat{g}(\eta;p) - g_0(\eta)\right] = p\hbar_g \mathbf{N}_g\left[\hat{f}(\eta;p), \hat{g}(\eta;p)\right], \tag{21}$$

$$(1-p)L_\theta\left[\hat{\theta}(\eta;p) - \theta_0(\eta)\right] = p\hbar_\theta \mathbf{N}_\theta\left[\hat{f}(\eta;p), \hat{g}(\eta;p), \hat{\theta}(\eta,p)\right], \tag{22}$$

$$\hat{f}(0;p)=0,\ \hat{f}'(0;p)=1,\ \hat{f}'(\infty;p)=0,$$
$$\hat{g}(0;p)=0,\ \hat{g}'(0;p)=\beta,\ \hat{g}'(\infty;p)=0, \quad (23)$$
$$\hat{\theta}(0,p)=1,\ \hat{\theta}(\infty,p)=0,$$

$$\mathbf{N}_f[\hat{f}(\eta,p),\hat{g}(\eta,p)]=\left(1+\frac{1}{\beta}\right)\frac{\partial^3\hat{f}(\eta,p)}{\partial\eta^3}$$
$$-\left(\frac{\partial\hat{f}(\eta,p)}{\partial\eta}\right)^2+(\hat{f}(\eta,p)+\hat{g}(\eta,p))\frac{\partial^2\hat{f}(\eta,p)}{\partial\eta^2}$$
$$-M^2\frac{\partial\hat{f}(\eta,p)}{\partial\eta}, \quad (24)$$

$$\mathbf{N}_g[\hat{g}(\eta,p),\hat{f}(\eta,p)]=\left(1+\frac{1}{\beta}\right)\frac{\partial^3\hat{g}(\eta,p)}{\partial\eta^3}$$
$$-\left(\frac{\partial\hat{g}(\eta,p)}{\partial\eta}\right)^2+(\hat{f}(\eta,p)+\hat{g}(\eta,p))\frac{\partial^2\hat{g}(\eta,p)}{\partial\eta^2}$$
$$-M^2\frac{\partial\hat{g}(\eta,p)}{\partial\eta}, \quad (25)$$

$$\mathbf{N}_\theta[\hat{\theta}(\eta,p),\hat{f}(\eta,p),\hat{g}(\eta,p)]=\frac{\partial^2\hat{\theta}(\eta,p)}{\partial\eta^2}$$
$$+\Pr(\hat{f}(\eta,p)+\hat{g}(\eta,p))\frac{\partial\hat{\theta}(\eta,p)}{\partial\eta}+\Pr B\hat{\theta}(\eta,p). \quad (26)$$

In above equations, p is an embedding parameter, $\hbar_f$, $\hbar_g$ and $\hbar_\theta$ the non-zero auxiliary parameters and $\mathbf{N}_f$, $\mathbf{N}_g$ and $\mathbf{N}_\theta$ the nonlinear operators. Setting $p=0$ and $p=1$ one has

$$\hat{f}(\eta;0)=f_0(\eta),\ \hat{\theta}(\eta,0)=\theta_0(\eta)$$
$$\text{and } \hat{f}(\eta;1)=f(\eta),\ \hat{\theta}(\eta,1)=\theta(\eta), \quad (27)$$

and when variation of p is taken from 0 to 1 then $f(\eta,p)$, $g(\eta,p)$ and $\theta(\eta,p)$ vary from $f_0(\eta)$, $g_0(\eta)$, $\theta_0(\eta)$ to $f(\eta)$, $g(\eta)$ and $\theta(\eta)$. Taylor's series expansion yields

$$f(\eta,p)=f_0(\eta)+\sum_{m=1}^{\infty}f_m(\eta)p^m, \quad (28)$$

$$g(\eta,p)=g_0(\eta)+\sum_{m=1}^{\infty}g_m(\eta)p^m, \quad (29)$$

$$\theta(\eta,p)=\theta_0(\eta)+\sum_{m=1}^{\infty}\theta_m(\eta)p^m, \quad (30)$$

$$f_m(\eta)=\frac{1}{m!}\frac{\partial^m f(\eta;p)}{\partial\eta^m}\bigg|_{p=0},$$
$$g_m(\eta)=\frac{1}{m!}\frac{\partial^m g(\eta;p)}{\partial\eta^m}\bigg|_{p=0},$$
$$\theta_m(\eta)=\frac{1}{m!}\frac{\partial^m\theta(\eta;p)}{\partial\eta^m}\bigg|_{p=0}. \quad (31)$$

Note that the convergence in the above series strongly depends upon $\hbar_f$, $\hbar_g$ and $\hbar_\theta$. Considering that $\hbar_f$, $\hbar_g$ and $\hbar_\theta$ are selected properly so that (28)-(30) converge at $p=1$. Therefore we have

$$f(\eta)=f_0(\eta)+\sum_{m=1}^{\infty}f_m(\eta), \quad (32)$$

$$g(\eta)=g_0(\eta)+\sum_{m=1}^{\infty}g_m(\eta), \quad (33)$$

$$\theta(\eta)=\theta_0(\eta)+\sum_{m=1}^{\infty}\theta_m(\eta). \quad (34)$$

We write the general solutions as follows

$$f_m(\eta)=f_m^*(\eta)+C_1+C_2e^{\eta}+C_3e^{-\eta}, \quad (35)$$

$$g_m(\eta)=g_m^*(\eta)+C_4+C_5e^{\eta}+C_6e^{-\eta}, \quad (36)$$

$$\theta_m(\eta)=\theta_m^*(\eta)+C_7e^{\eta}+C_8e^{-\eta}, \quad (37)$$

where f_m^*, g_m^* and θ_m^* are the special solutions.

4. CONVERGENCE ANALYSIS AND DISCUSSION

Eqs. (8)-(12) are solved by homotopy analysis method (HAM). HAM solution contains the auxiliary parameters $\hbar_f$, $\hbar_g$ and $\hbar_\theta$. These auxiliary parameters $\hbar_f$, $\hbar_g$ and $\hbar_\theta$ can adjust and control the convergence of the constructed series solutions. In order to find the range of admissible values of $\hbar_f$, $\hbar_g$ and $\hbar_\theta$, the $\hbar-$ curves are potrayed for 19*th* -order of approximations. Fig. 1 clearly shows that the range of admissible values of $\hbar_f$, $\hbar_g$ and $\hbar_\theta$ are $-1.15\le\hbar_f\le-0.05$, $-1.2\le\hbar_g\le-0.05$ and $-1.15\le\hbar_\theta\le-0.65$. The series converges in the whole region of η for $\hbar_f=\hbar_g-0.7$ and $\hbar_\theta=-0.9$.

Figs. 2 and 3 are presented to analyze the influences of Hartman number M and Casson fluid parameter β on the velocities $f'(\eta)$ and $g'(\eta)$. Figs. 2a and 2b describe the effects of Hartman number on the fluid velocities $f'(\eta)$ and $g'(\eta)$. The fluid velocities and their associated momentum boundary layer thicknesses are reduced with an increase in Hartman number.

Harman number has similar effects for the velocities $f'(\eta)$ and $g'(\eta)$. An increase in the Hartman number leads to a stronger Lorentz force.

Stronger Lorentz force creates a resistance in the fluid flow that appears in the reduction of velocities (see Figs. 2a and 2b).

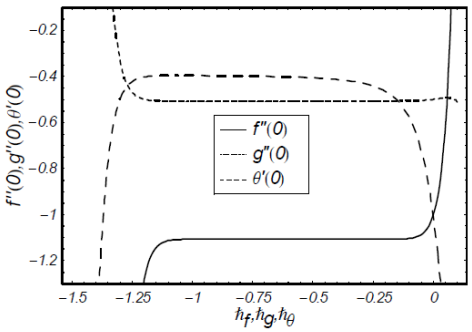

Fig. 1. $\hbar$ – **curves for the functions** f, g **and** θ **when** $M = 0.6$, $\beta = 1.5$, $\alpha = 0.5$, $\lambda = 2.0$, $\Pr = 0.9$ **and** $B = 0.3$.

Figs. 3a and 3b show that the larger values of Casson parameter β caused a decrease in the velocities $f'(\eta)$ and $g'(\eta)$. From these Figs. we analyzed that the fluid velocities and their associated momentum boundary layer thicknesses are decreasing functions of Casson parameter.

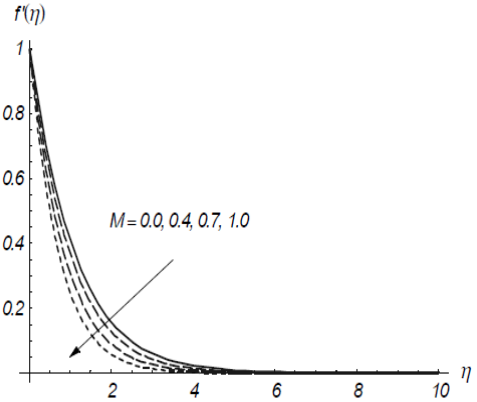

(a)

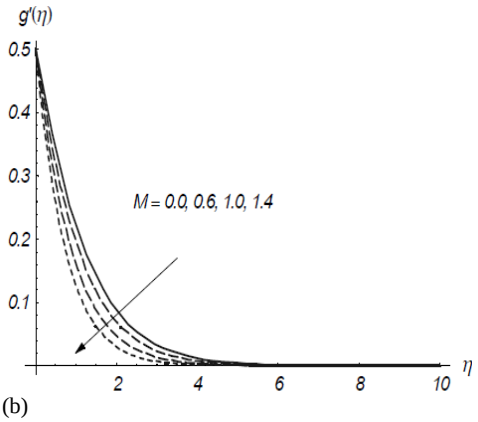

(b)

Fig. 2. (a) Influence of M **on** $f'(\eta)$ **and (b) for** $g'(\eta)$ **when** $\beta = 1.5$, $\lambda = 2.0$ **and** $\alpha = 0.5$.

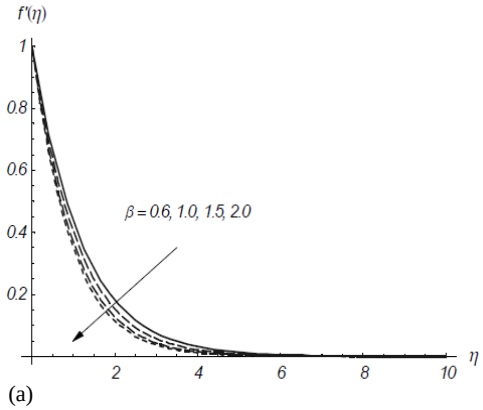

(a)

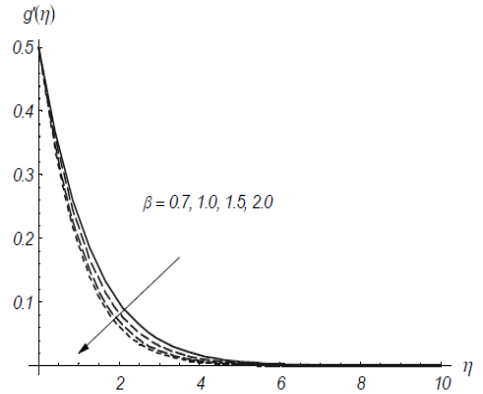

(b)

Fig. 3. (a) Influence of β **on** $f'(\eta)$ **and (b) for** $g'(\eta)$ **when** $M = 0.6$, $\lambda = 2.0$ **and** $\alpha = 0.5$.

To see the influences of ratio parameter α, Prandtl number $\Pr$, heat generation/absorption parameter B and porosity parameter on the temperature $\theta(\eta)$, Figs. 4 and 5 are sketched. Fig. 4a shows that the temperature $\theta(\eta)$ and thermal boundary layer thickness are increasing functions of ratio parameter α. Fig. 4b presents the variations of Prandtl number on the temperature. In this Fig. we have seen that the temperature and thermal boundary layer thickness are reduced for the larger Prandtl number. In fact the fluids with lower Prandtl number have higher thermal diffusivity. Higher thermal diffusivity gives rise to a decrease in temperature and lowers the thermal boundary layer thickness. The role of Prandtl number is to control the rate of cooling in conducting fluid. Fig. 5a is sketched to analyze the variations of heat generation/absorption parameter on the temperature. We have seen that an increase in B enhances the temperature and thermal boundary layer thickness. When heat generation parameter is increased, more heat is produced in the fluid that causes to a higher temperature and stronger thermal boundary layer thickness. Fig. 5b depicts the variation of porosity parameter on the temperature. An increase in porosity parameter shows a decrease in the temperature.

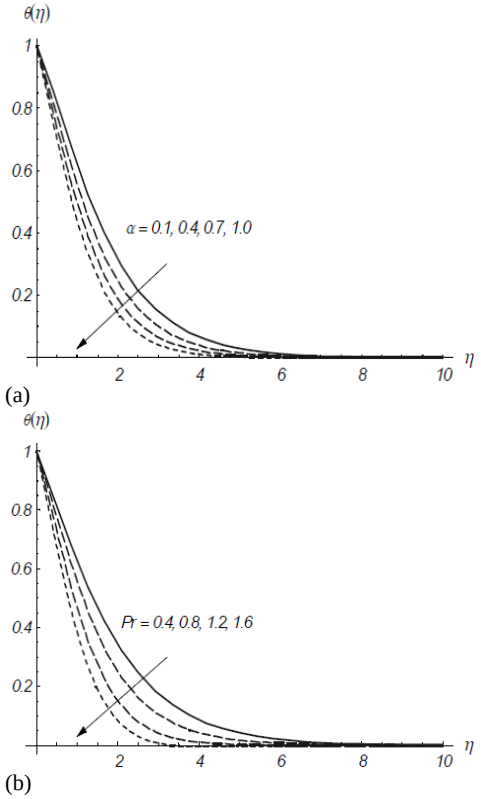

Fig. 4. (a) Influence of α on $\theta(\eta)$ when $M = 0.6$, $\beta = 1.5$, $\lambda = 2.0$, $\Pr = 0.9$ and $B = 0.4$. (b) Influence of $\Pr$ on $\theta(\eta)$ when $M = 0.6$, $\alpha = 0.5$, $\beta = 1.5$, $\lambda = 2.0$ and $B = 0.4$.

Figs. 6 and 7 are plotted to see the effects of different physical parameters on the skin-friction coefficients $-(1+1/\beta) f''(0)$, $-(1+1/\beta) g''(0)$ and local Nusselt number $-\theta'(0)$. Fig. 6a shows the effects of Hartman number vs Casson parameter on $-(1+1/\beta) f''(0)$. By increasing M and β, the skin-friction coefficients increases. It can be seen form Fig. 6b that Hartman number and Casson parameter have similar effects on $-(1+1/\beta) g''(0)$. A comparison of Figs. 6a and 6b shows that the skin-friction coefficient $-(1+1/\beta) f''(0)$ at the wall are greater than the skin-friction coefficient $-(1+1/\beta) g''(0)$.

A decrease in the local Nusselt number is noticed corresponds to the larger values of Hartman number vs Casson parameter (see Fig. 7a). From Fig. 7b we see that an increase in heat generation/absorption parameter leads to an increase in the local Nusselt number.

Figs. 8a and 8b show the variations in skin-friction coefficients $-(1+1/\beta) f''(0)$ and $-(1+1/\beta) g''(0)$ for different values of λ and α. Here we examined that the increasing values of λ and α lead a reduction in the skin-friction coefficients. From Figs. 9a and 9b, we observed that the local Nusselt number is an increasing function of λ, α and $\Pr$.

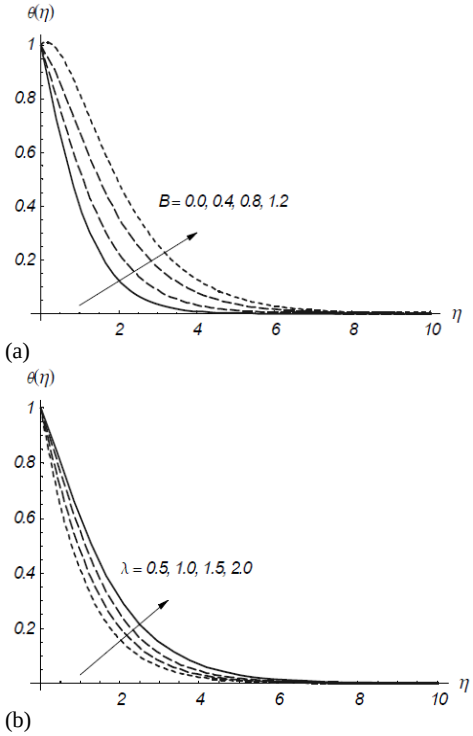

Fig. 5. (a) Influence of B on $\theta(\eta)$ when $M = 0.6$, $\beta = 1.5$, $\lambda = 2.0$, $\alpha = 0.5$ and $\Pr = 0.9$. (b) Influence of λ on $\theta(\eta)$ when $M = 0.6$, $\beta = 1.5$, $B = 0.3$, $\alpha = 0.5$ and $\Pr = 0.9$.

Table 1 is computed to analyze the numerical values of $f''(0)$, $g''(0)$ and $\theta'(0)$ for the fixed values of involved parameters. Here we have seen that the solutions for velocities converge from 10th order of approximation whereas the solution for temperature converges from 40th order of deformations. Table 2 is computed for the comparison values of $f''(0)$, $g''(0)$, $f(\infty)$ and $g(\infty)$ for different values of α when $\beta \to \infty$ and $M = 1/\lambda = 0$. This Table shows that our solutions in limiting situations have an excellent agreement with the previous study (Wang (1984).

5. CONCLUSIONS

The main results of present study can be summarized as follows:

- Hartman number M has quite opposite effects on the velocities and temperature.
- Casson fluid parameter β has similar behavior for the velocities $f'(\eta)$ and $g'(\eta)$ in a qualitative sense.
- Temperature increases by increasing in heat generation parameter B.

- Increase in porosity parameter decreases the fluid temperature.
- Skin-friction coefficient is increased for larger Casson fluid parameter.
- Local Nusselt number is an increasing function of B vs α.

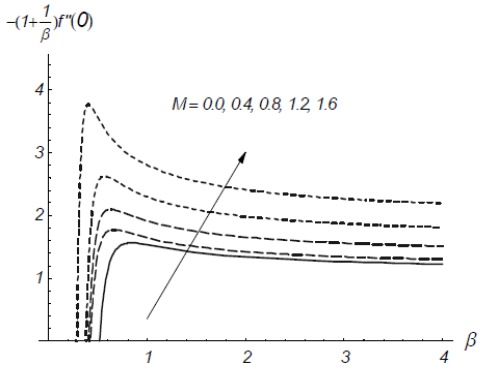

(a)

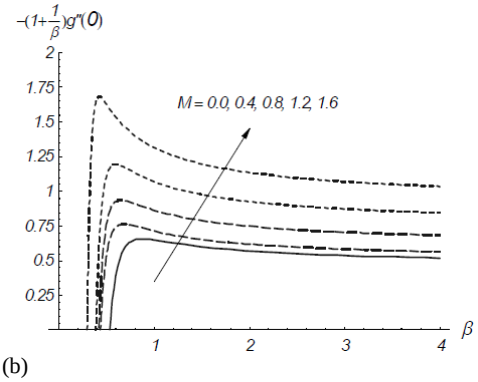

(b)

Fig. 6. (a) Effects of M vs β on $-\left(1+\frac{1}{\beta}\right)f''(0)$ and (b) for $-\left(1+\frac{1}{\beta}\right)g''(0)$ when $\alpha = 0.5$ and $\lambda = 2.0$.

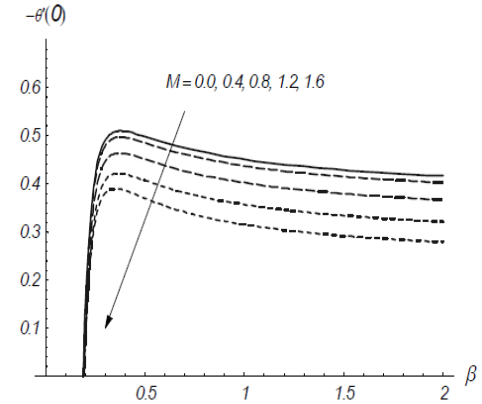

(a)

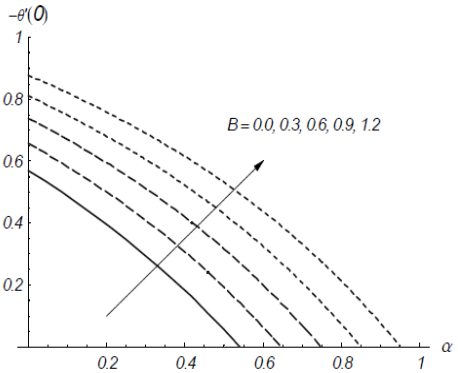

(b)

Fig. 7. (a) Effects of M vs β on $-\theta'(0)$ when $\alpha = 0.5$, $\lambda = 2.0$, $B = 0.3$ and $\Pr = 0.9$. (b) Effects B vs α on $-\theta'(0)$ when $M = 0.6$, $\lambda = 2.0$, $\beta = 1.5$ and $\Pr = 0.9$.

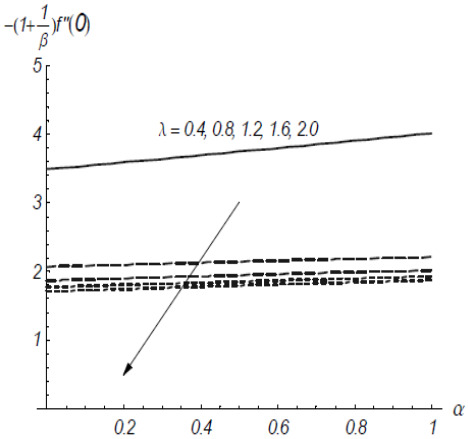

(a)

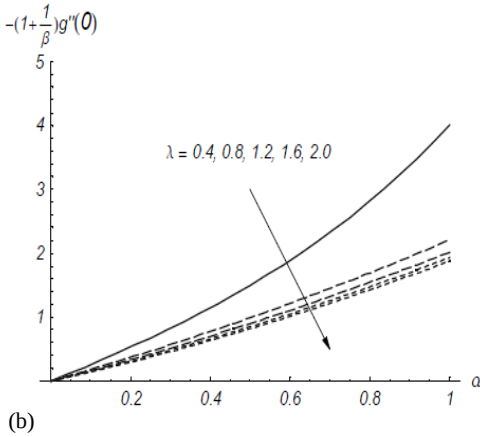

(b)

Fig. 8. (a) Effects of λ vs α on $-\left(1+\frac{1}{\beta}\right)f''(0)$ and (b) for $-\left(1+\frac{1}{\beta}\right)g''(0)$ when $M = 0.5$ and $\beta = 1.5$.

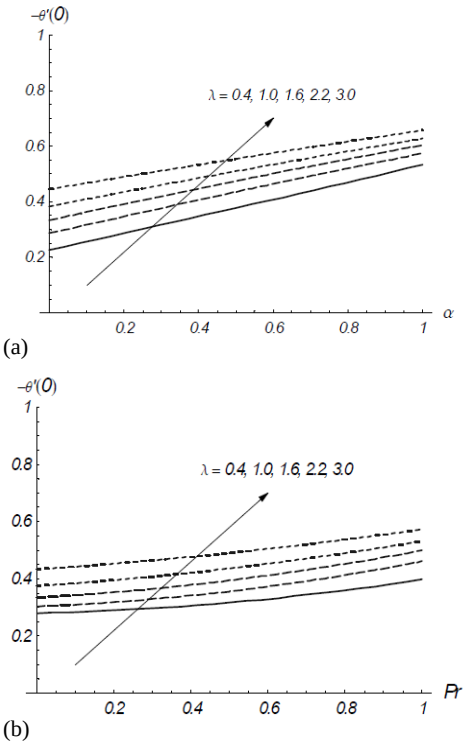

Fig. 9. (a) Effects of λ vs α on $-\theta'(0)$ when $M = 0.5$, $\beta = 1.5$, $B = 0.3$ and $\Pr = 0.9$. (b) Effects λ vs $\Pr$ on $-\theta'(0)$ when $M = 0.5 = \alpha$, $\beta = 1.5$ and $B = 0.3$.

Table 1 Convergence values of homotopic solutions for different order of deformations when $\beta = 1.5$, $\lambda = 2.0$, $M = 0.6$, $\alpha = 0.5$, $\Pr = 0.9$, $B = 0.3$, $\hbar_f = \hbar_g = -0.7$ and $\hbar_\theta = -0.9$.

Order of deformations	$-f''(0)$	$-g''(0)$	$-\theta'(0)$
01	1.126000	0.504667	0.63100
10	1.106868	0.506429	0.40657
20	1.106868	0.506429	0.39747
30	1.106868	0.506429	0.39619
40	1.106868	0.506429	0.39593
45	1.106868	0.506429	0.39593
50	1.106868	0.506429	0.39593

Table 2 Numerical values of $f''(0)$, $g''(0)$, $f(\infty)$ and $g(\infty)$ for different values of α when β, $\lambda \to \infty$ and $M = 0$.

	Wang (1984)			
α	$-f''(0)$	$-g''(0)$	$f(\infty)$	$g(\infty)$
0.0	1	0	1	0
0.25	1.0488	0.1945	0.9070	0.2579
0.50	1.0930	0.4652	0.8423	0.4516
0.75	1.1344	0.7946	0.7923	0.6120
1.0	1.1737	1.1737	0.7515	0.7515

Present results			
$f''(0)$	$g''(0)$	$f(\infty)$	$g(\infty)$
-1	0	1	0
-1.04881	-0.19457	0.907047	0.25790
-109309	-0.46522	0.84293	0.45169
-1.13450	-0.79462	0.79231	0.61214
-1.17372	-1.17372	0.75149	0.75149

REFERENCES

Abelman, S., E. Momoniat and T. Hayat (2009). Couette flow of a third grade fluid with rotating frame and slip condition. *Nonlinear Analysis: Real World Appl.* 10, 3329-3334.

Ariel, P. D (2003). Generalized three dimensional flow due to a stretching surface. *Z. Angew. Math. Mech.* 83, 844-852.

Bhattacharyya, K. and I. Pop (2011). MHD boundary layer flow due to an exponentially shrinking sheet. *Magnetohydrodynamics* 47, 337-344.

Chamkha, A. J. (1999). Hydromagnetic three-dimensional free convection on a vertical stretching surface with heat generation or absorption. *Int. J. Heat Fluid Flow* 20, 84-92.

Crane, L. J. (1970). Flow past a stretching plate. *Z. Angew. Math. Physk.* 21, 645-647.

Hayat, T., S. Asad and A. Alsaedi (2014d). Flow of variable thermal conductivity fluid due to inclined stretching cylinder with viscous dissipation and thermal radiation. *Appl. Math. Mech. 35, 717-728.*

Hayat, T., S. Asad M. Mustafa and A. Alsaedi (2014a). Radiation effects on the flow of Powell-Eyring fluid past an unsteady inclined stretching sheet with non-uniform heat source/sink. *Plos One* 9, e103214.

Hayat, T., S. Asad, M. Mustafa and H. H. Alsulami (2014b). Heat transfer analysis in the flow of Walters'B fluid with a convective boundary condition. *Chin. Phys. B* 23, 084701.

Hayat, T., R. Naz and M. Sajid (2010). On the homotopy solution for Poiseuille flow of a fourth grade fluid. *Commun. Nonlinear Sci. Numer. Simulat.* 15, 581-589.

Hayat, T., S. A. Shehzad and A. Alsaedi (2012c). Soret and Dufour effects in magnetohydrodynamic (MHD) flow of Casson fluid *Appl. Math. Mech.* 33, 1301-1312.

Hayat, T., S. A., Shehzad, S. Al-Mezel and A. Alsaedi (2014c). Three-dimensional flow of an Oldroyd-B fluid over a bidirectional stretching surface with prescribed surface temperature and prescribed surface heat flux. *J. Hydrol. Hydromech.* 62, 117-125.

Hayat, T., S. A. Shehzad, A. Alsaedi and M. S. Alhothuali (2012b). Mixed convection stagnation point flow of Casson fluid with convective boundary conditions. *Chin. Phys. Lett.* 29, 114704.

Hayat, T., Shehzad, S. A., M. Mustafa and A. A. Hendi (2012a). MHD flow of an Oldroyd-B fluid through a porous channel. *Int. J. Chem. Reactor Eng.* 10, A8.

Hayat, T., S. A. Shehzad, M. Qasim and A. Alsaedi (2012c). Radiative flow with variable thermal conductivity in porous medium. *Z. Naturforschung A* 67a, 153-159.

Jamil, M. and C. Fetecau (2010). Some exact solutions for rotating flows of a generalized Burgers' fluid in cylindrical domains. *J. Non-Newtonian Fluid Mech.* 165, 1700-1712.

Jamil, M., N. A. Khan and S. Nazish (2013). Fractional MHD Oldroyd-B fluid over an oscillating plate. *Thermal Sci.* 17, 997-1011.

Jamil, M., A. Rauf, C. Fetecau and N. A. Khan (2011). Helical flows of second grade fluid due to constantly accelerated shear stresses. *Commun. Nonlinear Sci. Numer. Simulat.* 16, 1959-1969.

Javed, T., M. Sajid, Z. Abbas and N. Ali (2011). Non-similar solution for rotating flow over an exponentially stretching surface. *Int. J. Num. Methods Heat Fluid Flow* 21, 903-908.

Liao, S.J (2003). Beyond perturbation: Introduction to homotopy analysis method. *Chapman and Hall, CRC Press, Boca Raton*.

Makinde, O. D. (2012). Computational modelling of MHD unsteady flow and heat transfer toward a flat plate with Navier slip and Newtonian heating, *Braz. J. Chem. Eng.* 29, 159-166.

Malvandi, A., F. Hedayati and M. R. H. Nobari (2014a). An analytical study on boundary layer flow and heat transfer of nanofluid induced by a non-linearly stretching sheet. *J. Appl. Fluid Mech.* 7, 375-384.

Malvandi, A., F. Hedayati and M. R. H. Nobari (2014b). An HAM analysis of stagnation-point flow of a nanofluid over a porous stretching sheet with heat generation. *J. Appl. Fluid Mech.* 7, 135-145.

Mukhophadhyay, S. (2012). Heat transfer analysis of the unsteady flow of a Maxwell fluid over a stretching surface in the presence of a heat source/sink. *Chin. Phys. Lett.* 29, 054703.

Rashidi, M. M. and E. Erfani (2012). Analytical method for solving steady MHD convective and slip flow due to a rotating disk with viscous dissipation and Ohmic heating. *Engin. Comput.* 29, 562-579.

Rashidi, M. M. and N. F. Mehr (2014). Series solutions for the flow in the vicinity of the equator of an MHD boundary-layer over a porous rotating sphere with heat transfer. *Thermal Sci.* 18, 527-537.

Rashidi, M. M., A. J. Chamkha and M. Keimanesh (2011). Application of multi-step differential transform method on flow of a second-grade fluid over a stretching or shrinking sheet. *American J. Comput. Math.* 6, 119-128.

Rashidi, M. M., S. A. M. Pour and S. Abbasbandy (2011). Analytic approximate solutions for heat transfer of a micropolar fluid through a porous medium with radiation, *Commun. Nonlinear Sci. Numer. Simulat.* 16, 1874-1889.

Shahmohamadi, H. (2012). Analytic study on non-Newtonian natural convection boundary layer flow with variable wall temperature on a horizontal plate. *Meccanica* 47, 1313-1323.

Shehzad, S. A., A. Alsaedi and T. Hayat (2012). Three dimensional flow of Jeffery fluid with convective boundary conditions. *Int. J. Heat Mass Transfer* 55, 3971-3976.

Shehzad, S. A., A. Alsaedi and T. Hayat (2013). Hydromagnetic steady flow of Maxwell fluid over a bidirectional stretching surface with prescribed surface temperature and prescribed surface heat flux. *Plos One* 8, e68139.

Shehzad, S. A., T. Hayat, M. S. Alhuthali and S. Asghar (2014). MHD three-dimensional flow of Jeffrey fluid with Newtonian heating. *J. Cent. South Uni.* 21, 1428-1433

Turkyilmazoglu, M. (2011). Numerical and analytical solutions for the flow and heat transfer near the equator of an MHD boundary layer over a porous rotating sphere. *Int. J. Thermal Sci.* 50, 831-842.

Turkyilmazoglu, M. (2012). Solution of the Thomas-Fermi equation with a convergent approach, *Commun. Nonlinear Sci. Numer. Simulat.* 17, 4097-4103.

Wang, C.Y (1984). The three-dimensional flow due to a stretching flat surface. *Phys. Fluids* 27, 1915-1917.

Wang, S. and W. C. Tan (2011). Stability analysis of soret-driven double-diffusive convection of Maxwell fluid in a porous medium. *Int. J. Heat Fluid Flow* 32, 88-94.